inorganics

MDPI

Article

Phenyl–Pentafluorophenyl Interaction-Mediated Ir(C^N)$_2$(N^N)-(Ni-Metallacycle) Dual Catalysis for Light-Driven C-S Cross-Coupling Synthesis

Jun-Feng Chen [1], Zhan-Xin Zhang [1], Jing Li [2,*] and Sheng-Li Huang [1,*]

[1] MOE Key Laboratory of Cluster Science, School of Chemistry and Chemical Engineering, Beijing Institute of Technology, Beijing 100081, China
[2] Technical Institute of Physics and Chemistry, Chinese Academy of Sciences, Beijing 100190, China
* Correspondence: lijingsp@mail.ipc.ac.cn (J.L.); huangsl@bit.edu.cn (S.-L.H.)

Abstract

In many photocatalytic systems employing dual catalysts, researchers often focus primarily on the individual performance of each catalyst while overlooking potential inter-catalyst interactions. In this work, we have developed an efficient dual-catalytic system for C-S cross-coupling reactions, utilizing Ir(C^N)$_2$(N^N) photosensitizers (PSs) in conjunction with Ni_3Ce metallacycles. By incorporating specifically designed ligands, we established phenyl–pentafluorophenyl interaction between the photosensitizer and the Ni_3Ce metallacycle. Comparative experiments revealed that systems featuring this interaction exhibited superior catalytic performance. Furthermore, transient fluorescence studies demonstrated that the phenyl–pentafluorophenyl interaction extends the lifetime of the excited state of the photosensitizer. The primary objective of this work is to provide some references and inspiration for the development of dual-catalytic systems.

Keywords: photocatalysis; dual catalysis; C-S cross-coupling; Ir(C^N)$_2$(N^N); phenyl–pentafluorophenyl interaction

check for updates

Academic Editors: Wolfgang Linert and Antonino Gulino

Received: 27 April 2025
Revised: 22 June 2025
Accepted: 3 July 2025
Published: 7 July 2025

Citation: Chen, J.-F.; Zhang, Z.-X.; Li, J.; Huang, S.-L. Phenyl–Pentafluorophenyl Interaction-Mediated Ir(C^N)$_2$(N^N)-(Ni-Metallacycle) Dual Catalysis for Light-Driven C-S Cross-Coupling Synthesis. *Inorganics* **2025**, *13*, 229. https://doi.org/10.3390/inorganics13070229

Copyright: © 2025 by the authors. Licensee MDPI, Basel, Switzerland. This article is an open access article distributed under the terms and conditions of the Creative Commons Attribution (CC BY) license (https://creativecommons.org/licenses/by/4.0/).

1. Introduction

Photochemical transformation has emerged as a compelling method for organic synthesis, distinguished by its unique reaction pathways compared to traditional thermal synthesis [1,2]. This approach not only facilitates the conversion of abundant solar energy into chemical energy but also allows for the creation of novel bonds that are often unattainable through nonphotochemical means, providing significant control over product specificity [3,4]. The formation of C-S bonds is particularly crucial for synthesizing functional molecules, including pharmaceuticals for cancer and HIV [5–7]. This contrasts with conventional thermal catalytic C-S cross-coupling reactions [8–11], which necessitate high temperatures and strong bases—thereby limiting functional group tolerance and product selectivity. The photochemical methods promote the generation of thiyl radicals, and this advancement enhances chemo-selectivity and broadens the scope of functional groups, accelerating the development of photochemical C-S bond synthesis [12,13].

The integration of photoredox and organometallic catalysts represents a significant advance in enhancing cross-coupling reactions [14–17]. This dual-catalysis approach typically involves a photosensitizer (PS) that absorbs light and modulates the oxidation states of the metal, leading to the formation of reactive intermediates. While the Ir/Ni dual-catalytic framework has been successfully applied to carbon–heteroatom cross-coupling [18–20],

the reaction efficiency often suffers from inadequate charge transfer between the PS and catalyst. Addressing this issue through direct covalent or coordination links can enhance charge transfer and reduce recombination. Furthermore, the incorporation of supramolecular interactions, such as host–guest and hydrogen bonding, presents a promising avenue for improving charge transfer efficiency [21–25]. Notably, the phenyl–pentafluorophenyl interaction, characterized by its unique electrostatic properties and molecular stacking arrangements [26–28], has potential applications in optimizing photocatalytic systems, although reports on its influence in this area remain limited.

Metallasupramolecules have garnered significant interest due to their unique structures and functional advantages, facilitating the development of diverse molecular architectures with tailored properties [29–32]. A prominent area of focus is the advancement of flask-like catalytic prototypes, which exhibit remarkable suprastructures and catalytic characteristics [33–35]. Notably, a novel [3 + 3] Schiff base macrocycle [36] that features three N_2O_2 salphen-type binding sites serves as a macrocyclic tris(salen) ligand, enabling the formation of a new family of heterometallic catalysts. These catalysts offer tunable performance through the manipulation of metal ions at the salen and trimetal crown ether sites. This study highlights the successful integration of an $Ir(C^N)_2(N^N)$ PS with a heterotetranuclear $LnNi_3$ complex (Figure 1), utilizing the pentafluorophenyl–phenyl interaction (as shown in Figure 2, which is a schematic diagram created using Material Studio [37] to illustrate the interaction site, and is not based on DFT calculations or crystallographic data) to achieve exceptional photocatalytic activity in C-S cross-coupling reactions.

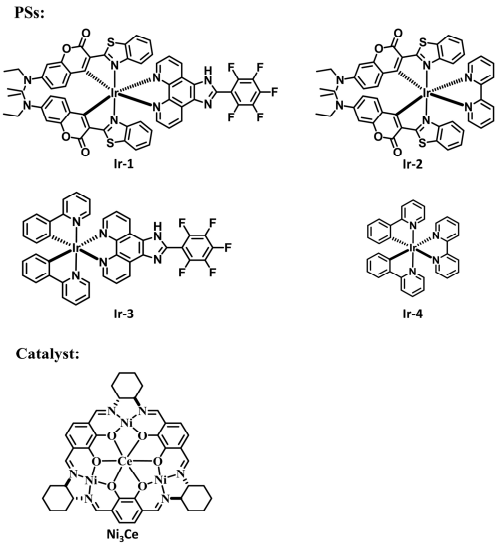

Figure 1. Structures of PSs and the catalyst used in this study.

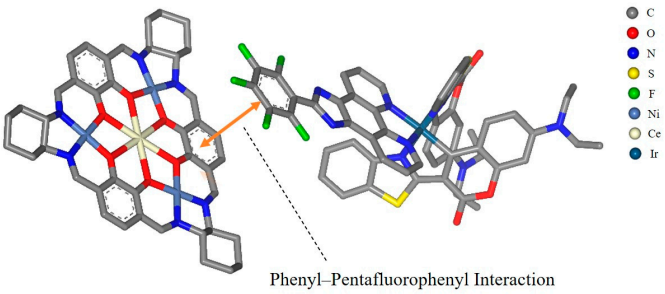

Figure 2. Phenyl–pentafluorophenyl interaction between Ni_3Ce (left) and Ir-1 (right). All hydrogen atoms are omitted for clarity. This figure was created using BIOVIA Materials Studio 2020.

2. Results

2.1. Fourier-Transform Infrared Spectroscopy of Ni_3Ce

This study investigated the impact of phenyl–pentafluorophenyl interactions between different PSs and Ni_3Ce catalysts on the C-S cross-coupling reaction. The synthesis of four PSs, namely Ir-1, Ir-2, Ir-3, and Ir-4, and Ni_3Ce was confirmed through ^1H NMR and ESI-MS (the figure is provided in the Supplementary Materials). For Ni_3Ce, Fourier-transform infrared (FTIR) spectroscopy (Figure 3) further confirmed its synthesis, in which there were no peaks indicative of unreacted aldehyde or amino groups, thus confirming the complete conversion of the starting materials. Characteristic peaks at 1614 cm^{-1} and 1465 cm^{-1} in the FTIR spectra correspond to the C=N bond. The peak at 1365 cm^{-1} and 1249 cm^{-1} correspond to the stretching vibrations of the C=N and C-O bonds, respectively. The peak at 774 cm^{-1} corresponds to the out-of-plane bending vibration of C-H on the benzene.

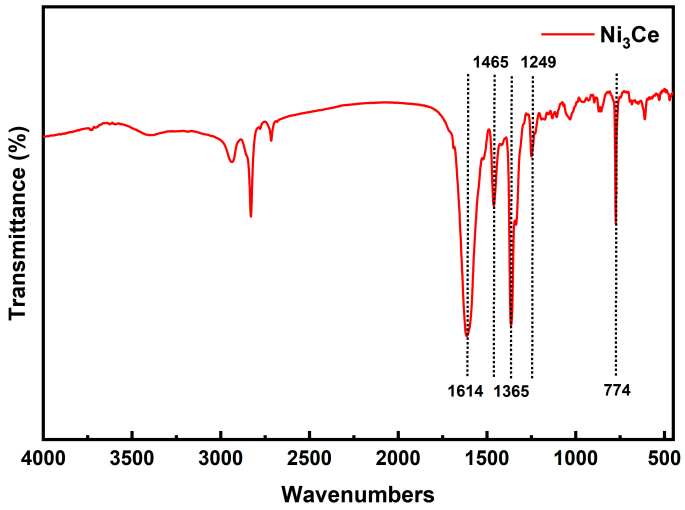

Figure 3. FT-IR spectra of Ni_3Ce.

2.2. Electrochemical Characterization of Ni_3Ce and Ir-Pss

The investigation of redox potentials for Ir-1, Ir-2, Ir-3, Ir-4, and Ni_3Ce substantiates the thermodynamic viability of electron transfer from the Ir-PS to the Ni catalyst. As illustrated in Figure 4, the cyclic voltammogram of Ni_3Ce reveals two distinct reduction potentials: E_{red1} at −0.62 V, attributed to the Ni^{2+}/Ni^{+} transition, and E_{red2} at −1.56 V, linked to the Ni^{+}/Ni^{0} transition. Each Ir-PS exhibits a series of reduction potentials indicative of their electron transfer capabilities; for instance, Ir-1 presents three reduction potentials at −0.87 V, −1.11 V, and −1.30 V, correlating with its respective oxidation states. Similar observations are made for Ir-2, Ir-3, and Ir-4, confirming their ability to reduce Ni^{2+} to Ni^{+}, yet highlighting their incapacity to further reduce Ni^{+} to Ni^{0}. This analysis underscores the potential utility of these Ir-PSs in catalytic applications involving nickel species.

2.3. Photocatalytic C-S Cross-Coupling Reaction Studies

This study investigates the role of phenyl–pentafluorophenyl interactions in enhancing photocatalysis within C-S cross-coupling reactions. Initially, PS Ir-1, incorporating coumarin and pentafluorophenyl moieties, demonstrated significant light absorption and synergy with phenyl groups. Our experimental focus on the reaction between 1-iodo-4-(trifluoromethyl)benzene and 4-methylbenzenethiol, facilitated by pyridine at ambient temperature, yielded an exceptional 99% (Table 1, entry 1). Crucially, both light and catalyst presence were essential, as omitting either resulted in negligible reaction. The absence of base decreased the yield to 80%, while oxidative coupling under air condi-

tions reduced it further to 33% (entries 2–6). Substituting Ir-1 for Ir-2 yielded only 75% (entry 7), attributed to absent phenyl–pentafluorophenyl interactions. Utilizing Ir-3, despite its pentafluorophenyl content, resulted in only 82% yield (entry 8), lower than Ir-1 due to decreased light absorption. Notably, Ir-4 performed even poorer at 52% (entry 9), underscoring the significance of these interactions. Thus, the phenyl–pentafluorophenyl interaction emerges as a crucial factor, enhancing electron transfer efficiency and, consequently, overall reaction conversion.

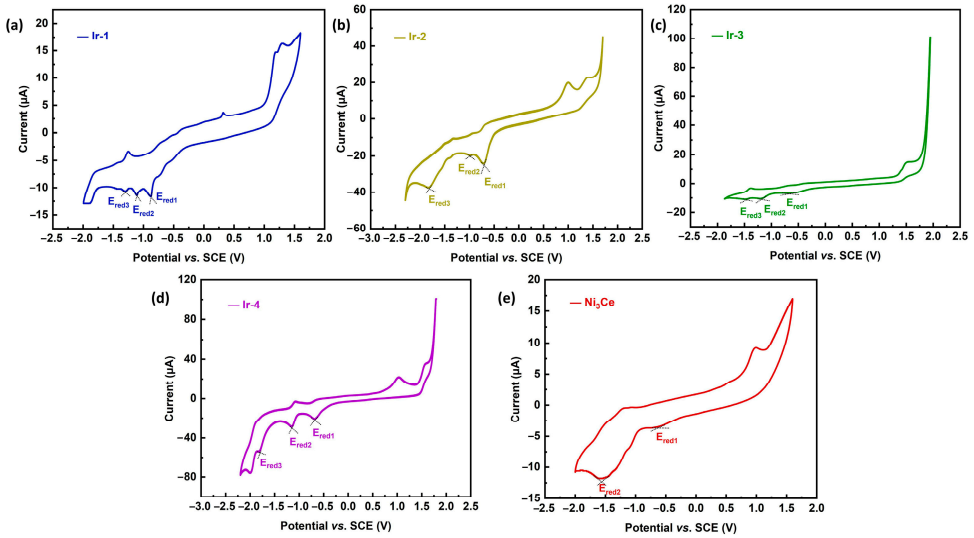

Figure 4. CVs of (**a**) Ir-1, (**b**) Ir-2, (**c**) Ir-3, (**d**) Ir-4 and (**e**) Ni_3Ce. Conditions: compounds (1 mM), $TBAPF_6$ (0.1 M), scan rate 50 $mV \cdot s^{-1}$. Glassy carbon working electrode, saturated calomel electrode (SCE) reference electrode, and platinum foil counter electrode.

Table 1. Effect of different conditions on photocatalytic C-S cross-coupling reaction.

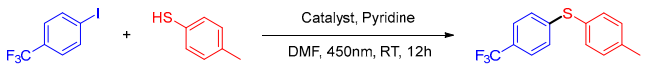

Entry	Variation from Standard Conditions [a]	Yield [b] (%)
1	Ir-1	99
2	No Ir-1	N.D.
3	No Ni_3Ce	N.D.
4	No light	N.D.
5	No base	80
6	Air	33
7	Ir-2	75
8	Ir-3	82
9	Ir-4	52

[a] Standard conditions: 1-iodo-4-(trifluoromethyl)benzene (0.1 mmol), 4-methylbenzenethiol (0.15 mmol), Ni_3Ce (0.00165 mmol), Ir-PS (0.00165 mmol), pyridine (0.15 mmol), 0.5 mL DMF, under N_2 atmosphere, 10 W 450 nm LED lamp. [b] Yield was determined using GC-MS. N.D.: not detected.

To further investigate our hypothesis, we conducted steady-state emission (Figure S2) and fluorescence titrations (Figure 5) of Ir-1, Ir-2, and Ir-3. Our findings, along with previous reports [38,39], indicate that the emission peaks at 516 nm for both Ir-1 and Ir-2 arise from the coumarin 6-localized excited state (^{3}LC), while the peaks at 574 nm for Ir-1 and 583 nm for Ir-2 correspond to the Ir^{III} excited state (MLCT). Notably, fluorescence titration of Ir-1 revealed a significant intensity enhancement at 574 nm, and Ir-3 similarly displayed a pronounced fluorescence enhancement, attributed to the phenyl–pentafluorophenyl

interaction with Ni_3Ce, which extended the excited-state lifetime of Ir-1 and promotes radiative transitions. This was further corroborated by fluorescence lifetime measurements (Figure 6), where Ir-1′s lifetime increased from 105 ns to 117 ns with rising Ni_3Ce concentration, whereas Ir-2′s lifetime experienced only a minor decrease from 84 ns to 81 ns. These results underscore the distinct intermolecular interactions between Ni_3Ce and Ir-1, highlighting Ir-1′s unique structural properties that enhance its fluorescence response.

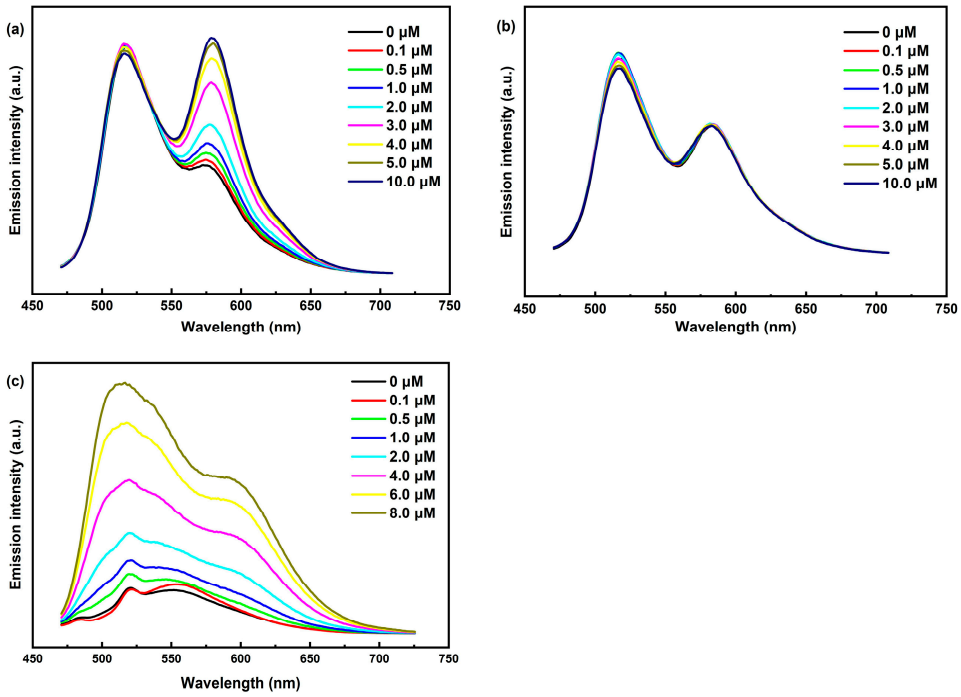

Figure 5. (**a**) Steady-state fluorescence titration of Ir-1 with Ni_3Ce. (**b**) Steady-state fluorescence titration of Ir-2 with Ni_3Ce. (**c**) Steady-state fluorescence titration of Ir-3 with Ni_3Ce. Conditions: 450 nm excitation, 25 μM Ir-Ps in DMF.

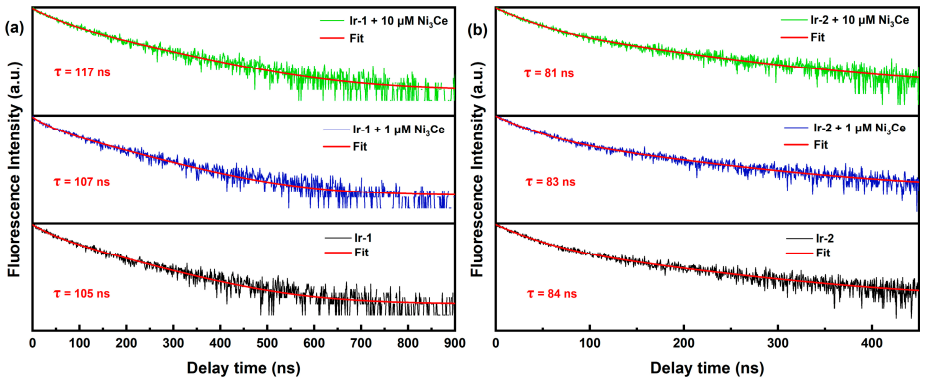

Figure 6. (**a**) Normalized luminescence decay kinetics of Ir-1 with different concentrations of Ni_3Ce. (**b**) Normalized luminescence decay kinetics of Ir-2 with different concentrations of Ni_3Ce. Conditions: 450 nm excitation, 25 μM Ir-1 (or Ir-2). The red curves are fits according to double exponential decay. The *y*-axis is in log scale.

The catalytic properties of the Ni_3Ce and Ir-1 system were rigorously evaluated under standard conditions (Scheme 1), revealing that the presence of electron-withdrawing groups on thiols significantly enhances the conversion rates in the C-S cross-coupling reaction. This phenomenon is attributed to the weakening of the C-I bond, facilitating the oxidative addition with nickel ions. While alterations to the thiol groups did not markedly impact

product yields, optimal results were achieved with substrates such as benzyl mercaptan and cyclohexanethiol, which exhibit favorable electronic characteristics. In conjunction with the redox potential of Ir-1 and previous reports [13], we propose a reaction mechanism for the system as illustrated in Figure 7. Upon irradiation with visible light, Ir-1 is excited to the Ir^{III*} state, which subsequently participates in a single electron transfer with thiols. This interaction results in the formation of Ir^{II} and a thiol radical cation, highlighting the intricate dynamics of this photochemical process. The reaction mechanism, supported by fluorescence quenching experiments (Figure S3) and the Stern–Volmer analysis ($I_0/I = 1 + K_{SV}[Q]$) yielding a K_{SV} of 16.4 M^{-1}, confirmed that thiols effectively quench the excited state of Ir-1. In this reaction sequence, pyridine facilitates the deprotonation of a thiol radical cation, yielding a thiyl radical. Concurrently, Ir^{II} reduces Ni^{2+} on Ni_3Ce to form Ni^+. The thiyl radical swiftly reacts with Ni^+ to generate a Ni^{2+}-SR complex, which is further reduced by Ir^{II}, regenerating Ir^{III}. The resulting Ni^+-SR undergoes oxidative addition with an aryl iodide, followed by a reductive elimination step that produces Ni^+ and the final product, Ar-SR.

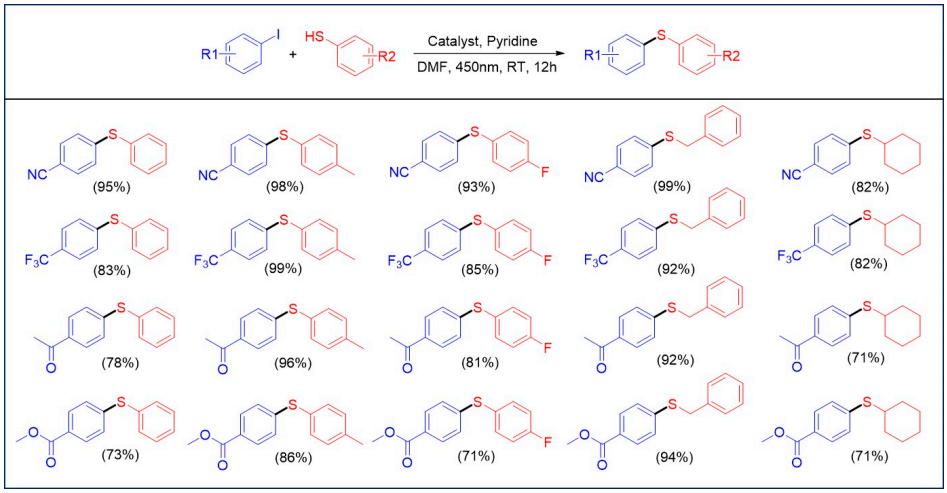

Scheme 1. Substrate scopes for C-S cross-coupling under standard conditions. Standard conditions: aryl iodide (0.1 mmol), thiols (0.15 mmol), Ni_3Ce (0.00165 mmol), Ir-1 (0.00165 mmol), pyridine (0.15 mmol), 0.5 mL DMF, under N_2 atmosphere, 10 W 450 nm LED lamp. Yield was determined using GC-MS.

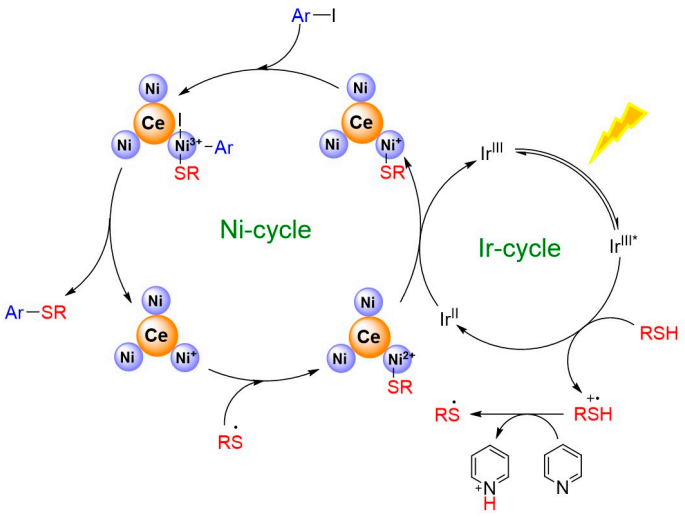

Figure 7. Proposed mechanism for photocatalytic C-S cross-coupling in this system. * representing excited state.

3. Materials and Methods

3.1. Reagents and Chemicals

The reagents used were as follows: 2,3-dihydroxyterephthalaldehyde ($C_8H_6O_4$, Energy Chemical, >99.9%, Pudong New District, Shanghai, China), cerium(III) acetate sesquihydrate ($Ce(OAc)_3{\cdot}nH_2O$, Energy Chemical, >99.9%, Pudong New District, Shanghai, China), nickel(II) acetate tetrahydrate ($Ni(OAc)_2{\cdot}4H_2O$, Energy Chemical, >99.9%, Pudong New District, Shanghai, China), (1R,2R)-(-)-1,2-cyclohexanediamine ($C_6H_{14}N_2$, Energy Chemical, >99.9%, Pudong New District, Shanghai, China), 1,10-phenanthroline-5,6-dione ($C_{12}H_6N_2O_2$, Energy Chemical, >99.9%, Pudong New District, Shanghai, China), pentafluorobenzaldehyde (C_7HF_5O, Energy Chemical, >99.9%, Pudong New District, Shanghai, China), ammonium acetate ($C_2H_7O_2N$, Energy Chemical, >99.9%, Pudong New District, Shanghai, China), iridium(III) chloride hydrate ($IrCl_3{\cdot}nH_2O$, Energy Chemical, >99.9%, Pudong New District, Shanghai, China), coumarin 6 ($C_{20}H_{18}N_2O_2S$, Energy Chemical, >99.9%, Pudong New District, Shanghai, China), 2,2′-bipyridine ($C_{10}H_8N_2$, Energy Chemical, >99.9%, Pudong New District, Shanghai, China), 2-phenylpyridine ($C_{11}H_9N$, Energy Chemical, >99.9%, Pudong New District, Shanghai, China), ammonium hydroxide (NH_5O, Energy Chemical, 25% in water, Pudong New District, Shanghai, China), ammonium hexafluorophosphate (NH_4PF_6, Energy Chemical, >99.9%, Pudong New District, Shanghai, China), 4-toluenethiol (C_7H_8S, Energy Chemical, >99.9%, Pudong New District, Shanghai, China), p-fluorothiophenol (C_6H_5FS, Energy Chemical, >99.9%, Pudong New District, Shanghai, China), benzyl mercaptan (C_7H_8S, Energy Chemical, >99.9%, Pudong New District, Shanghai, China), cyclohexanethiol ($C_6H_{12}S$, Energy Chemical, >99.9%, Pudong New District, Shanghai, China), 4-iodobenzotrifluoride ($C_7H_4F_3I$, Energy Chemical, >99.9%, Pudong New District, Shanghai, China), 4-iodobenzonitrile (C_7H_4IN, Energy Chemical, >99.9%, Pudong New District, Shanghai, China), 4′-iodoacetophenone (C_8H_7IO, Energy Chemical, >99.9%, Pudong New District, Shanghai, China), and methyl 4-iodobenzoate ($C_8H_7IO_2$, Energy Chemical, >99.9%, Pudong New District, Shanghai, China). All solvents and $Ir(ppy)_2(bpy)(PF_6)$ (Ir-4) were purchased from Tansoole (Xuhui District, Shanghai, China) and used without further purification.

3.2. Synthesis of Ni_3Ce

Synthesis of Ni_3Ce was carried out with reference to the procedure outlined in the literature [36]. A mixture of 2,3-dihydroxybenzene-1,4-dicarbaldehyde (149.4 mg, 0.9 mmol) and $Ce(OAc)_3{\cdot}nH_2O$ (95.1 mg, 0.3 mmol) in methanol (20 mL) was stirred at 70 °C under N_2 atmosphere. After stirring at 70 °C for 2 h, $Ni(OAc)_2{\cdot}4H_2O$ (223.9 mg, 0.9 mmol) was added and the mixture was stirred at 70 °C for 2 h. To the reaction mixture, a solution of (1R,2R)-(-)-1,2-diaminocyclohexane (102.7 mg, 0.9 mmol) in methanol was added and stirred at 70 °C for 24 h. After the reaction, the solvent was evaporated and the residue was recrystallized from methanol/diethyl ether. A brown solid was collected (292.1 mg, 80%). ^{1}H NMR (500 MHz, methanol-d_4): δ = 8.22 (s, 6H), 7.24 (s, 6H), 3.48 (br s, 6H), 2.78 (d, J = 9.5 Hz, 6H), 2.59 (br s, 9H), 2.01 (d, J = 4.5 Hz, 6H), 1.61 (m, 6H), 1.50 (m, 6H). MS (ESI^+) m/z: 1196.08 ($[Ni_3Ce]^+ + 2H_2O$).

3.3. Synthesis of 2-(2,3,4,5,6-Pentafluorophenyl)-1H-imidazo [4,5-F][1,10]phenanthroline (ppipH)

A mixture of 1,10-phenanthroline-5,6-dione (420.4 mg, 2 mmol), pentafluorobenzaldehyde (404.2 mg, 1 mmol), and ammonium acetate (3083.2 mg, 40 mmol) in acetic acid (15 mL) was stirred at 120 °C for 12 h under N_2 atmosphere. After the reaction, the mixture was poured into ice water and the pH of the mixture was adjusted to 7.0 by adding concentrated ammonia dropwise. The crude product was obtained by filtration, then washed with water and purified by recrystallization from ethanol/diethyl ether. A pink solid

was collected (478.8 mg, 62%). ^{1}H NMR (400 MHz, DMSO-d_6): δ = 14.27 (s, 1H), 9.09 (d, J = 4.4 Hz, 2H), 8.90 (d, J = 8.4 Hz, 2H), 7.87 (q, J = 4.0 Hz, 2H).

3.4. Synthesis of [Ir(coum)$_2$(ppipH)](PF$_6$) (Ir-1)

A mixture of $IrCl_3 \cdot nH_2O$ (350 mg, 1 mmol) and coumarin 6 (735.2 mg, 2.1 mmol) in 2-ethoxyethanol/water (20 mL, 1:1 *v*/*v*) was stirred at 120 °C for 60 h under N_2 atmosphere. After the reaction, the mixture was cooled to room temperature. Then, the precipitate was filtered off and washed with ethanol. The orange solid $[Ir(coum)_2Cl]_2$ was collected (787.5 mg, 85%).

A mixture of $[Ir(coum)_2Cl]_2$ (185.3 mg, 0.1 mmol) and ppipH (81.1 mg, 0.21 mmol) in DMA (10 mL) was stirred at 80 °C for 12 h under N_2 atmosphere. After cooling the reaction mixture to room temperature, NH_4PF_6 (195.6 mg, 1.2 mmol) was added and stirred for 1 h. The precipitate was removed by filtration and the concentrated filtrate was dropped into diethyl ether. The orange solid [Ir(coum)$_2$(ppipH)](PF$_6$) was collected (216.2 mg, 76%). ^{1}H NMR (400 MHz, DMSO-d_6): δ = 9.11 (d, J = 8.0 Hz, 2H), δ = 9.04 (d, J = 4.8 Hz, 2H), δ = 8.15 (dd, J = 8.0 and 5.2 Hz, 2H), δ = 7.99 (d, J = 7.6 Hz, 2H), 7.08 (t, J = 7.6 Hz, 2H), δ = 6.75 (t, J = 8.0 Hz, 2H), δ = 6.51 (d, J = 2.4 Hz, 2H), δ = 6.12 (d, J = 9.6 Hz, 2H), δ = 6.05 (d, J = 9.2 Hz, 2H), δ = 5.69 (d, J = 8.4 Hz, 2H), δ = 3.30 (q, J = 7.6 Hz, 8H), δ = 0.97 (t, J = 7.2 Hz, 12H). MS (ESI$^+$) *m*/*z*: 1277.22 ([Ir(coum)$_2$(ppipH)]$^+$).

3.5. Synthesis of [Ir(coum)$_2$(bpy)](PF$_6$) (Ir-2)

Synthesis of [Ir(coum)$_2$(bpy)](PF$_6$) was carried out with reference to the procedure in the literature [37]. A mixture of $IrCl_3 \cdot nH_2O$ (350 mg, 1 mmol) and coumarin 6 (735.2 mg, 2.1 mmol) in 2-ethoxyethanol/water (20 mL, 1:1 *v*/*v*) was stirred at 120 °C for 60 h under N_2 atmosphere. After the reaction, the mixture was cooled to room temperature. Then, the precipitate was filtered off and washed with ethanol. The orange solid $[Ir(coum)_2Cl]_2$ was collected (787.5 mg, 85%).

A mixture of $[Ir(coum)_2Cl]_2$ (185.3 mg, 0.1 mmol) and 2,2′-bipyridine (32.8 mg, 0.21 mmol) in DMA (10 mL) was stirred at 80 °C for 12 h under N_2 atmosphere. After cooling the reaction mixture to room temperature, NH_4PF_6 (195.6 mg, 1.2 mmol) was added and stirred for 1 h. The precipitate was removed by filtration and the concentrated filtrate was dropped into diethyl ether. The orange solid [Ir(coum)$_2$(bpy)](PF$_6$) was collected (198.5 mg, 83%). ^{1}H NMR (400 MHz, DMSO-d_6): δ = 8.80 (d, J = 5.2 Hz, 2H), δ = 8.64 (d, J = 8.4 Hz, 2H), δ = 8.31 (t, J = 7.6 Hz, 2H), δ = 8.11 (d, J = 8.0 Hz, 2H), 7.87 (t, J = 6.4 Hz, 2H), δ = 7.27 (t, J = 7.6 Hz, 2H), δ = 6.97 (t, J = 8.0 Hz, 2H), δ = 6.47 (s, 2H), δ = 6.03 (s, 4H), δ = 5.82 (d, J = 8.4 Hz, 2H), δ = 3.30 (q, J = 7.6 Hz, 8H), δ = 0.97 (t, J = 7.2 Hz, 12H).

3.6. Synthesis of [Ir(ppy)$_2$(ppipH)](PF$_6$) (Ir-3)

A mixture of $IrCl_3 \cdot nH_2O$ (350 mg, 1 mmol) and 2-phenylpyridine (325.9 mg, 2.1 mmol) in 2-ethoxyethanol/water (20 mL, 1:1 *v*/*v*) was stirred at 120 °C for 60 h under N_2 atmosphere. After the reaction, the mixture was cooled to room temperature. Then, the precipitate was filtered off and washed with ethanol. The orange solid $[Ir(ppy)_2Cl]_2$ was collected (509.2 mg, 95%).

A mixture of $[Ir(ppy)_2Cl]_2$ (185.3 mg, 0.1 mmol) and ppipH (81.1 mg, 0.21 mmol) in DMA (10 mL) was stirred at 80 °C for 12 h under N_2 atmosphere. After cooling the reaction mixture to room temperature, NH_4PF_6 (195.6 mg, 1.2 mmol) was added and stirred for 1 h. The precipitate was removed by filtration and the concentrated filtrate was dropped into diethyl ether. The orange solid [Ir(coum)$_2$(bpy)](PF$_6$) was collected (194.3 mg, 82%). ^{1}H NMR (400 MHz, DMSO-d6): δ = 9.17 (d, J = 8.4 Hz, 2H), δ = 8.27 (d, J = 8.0 Hz, 2H), δ = 8.20 (dd, J = 4.8 and 1.2 Hz, 2H), δ = 8.11 (dd, J = 8.0 and 5.2 Hz, 2H), δ = 7.96 (d, J = 7.2 Hz, 2H), δ = 7.89 (td, J = 7.6 and 1.2 Hz, 2H), δ = 7.53 (d, J = 5.2 Hz, 2H), δ = 7.07 (td, J = 7.6 and

0.8 Hz, 2H), δ = 6.97 (qd, J = 7.2 and 1.2 Hz, 4H), δ = 6.30 (d, J = 7.2 Hz, 2H). MS (ESI+) m/z: 887.15 ([Ir(ppy)2(ppipH)]$^+$).

3.7. Material Characterization

The synthesized materials were characterized using various advanced techniques. ^{1}H-NMR spectra were recorded at ambient temperature, unless otherwise stated, with a Bruker 500 MHz spectrometer(Bruker Corporation, Karlsruhe, Germany). All spectra were referenced to the corresponding solvent residual signal, i.e., 2.500 ppm for dimethyl sulfoxide, 1.940 ppm for acetonitrile, 7.260 for chloroform, 5.320 for dichloromethane, and 4.870 for methanol. Fourier-transform infrared (FT-IR) spectra were recorded in transmission mode on a Smart Omni-Transmission spectrometer (Thermo Fisher Scientific Inc., Waltham, MA, USA) using KBr pellets in the range 400~4000 cm^{-1}. Signals are given as wave numbers in cm-1 using the following abbreviations: vs. = very strong, s = strong, m = medium, w = weak, and b = broad. The C-S cross-coupling reaction was monitored by a GC (Shimadzu Corporation, Kyoto, Japan)) equipped with a HP-5 column, air carrier gas, and FID conductivity detector. The product was further confirmed via gas chromatography–mass spectrometry (GC-MS) using an Agilent 7890A/5975C. UV-Vis spectroscopy was performed on a TU-1901 spectrophotometer (Persee General Instrument Co. Ltd., Beijing, China). Steady-state emission spectroscopy was performed on an F-7000 fluorescence light spectrophotometer (Hitachi High-Tech Corporation, Tokyo, Japan). All systems were used with standard quartz cuvettes (d = 10.0 mm). An electrochemical test was performed on a CHI 760E electrochemical workstation (CH Instruments Inc., Shanghai, China). The electrochemical measurements were taken using a standard three-electrode system comprising a glassy carbon electrode (working electrode), a platinum foil electrode (counter electrode), and a saturated calomel electrode (reference electrode). Tetrabutylammonium hexafluorophosphate (0.1 M) served as the electrolyte in anhydrous DMF solutions of the compound (1.0 mM). All experiments were performed under a nitrogen atmosphere with a scan rate of 50 mV·s^{-1}. Electrospray ionization mass spectra (ESI-MS) were recorded on a liquid chromatography–mass spectrometer (AGILENT Q-TOF 6520). Time-resolved emission spectra were measured by an FLS-1000 photoluminescence spectrometer. Photocatalytic reactions were carried out using a multi-channel photochemical reaction system featuring 10 W 450 nm LED lamps.

3.8. General Procedure for the Photocatalytic Process

Under a N_2 atmosphere, 0.00165 mmol Ni_3Ce, 0.00165 mmol Ir-1, 0.1 mmol aryl iodide, 0.15 mmol thiols, 0.15 mmol pyridine, and 0.5 mL DMF were added into a 10 mL photocatalytic bottle, under irradiation of a 10 W 450 nm LED lamp for 12 h at room temperature. Conversions were determined by gas chromatography.

4. Conclusions

In conclusion, we have successfully developed an efficient dual-catalytic C-S cross-coupling reaction system utilizing Ir(CˆN)$_2$(NˆN) PSs and a Ni_3Ce metallacycle. By incorporating specific ligands, we established a phenyl–pentafluorophenyl interaction between the PS and the Ni_3Ce metallacycle, significantly enhancing the conversion rates of the C-S cross-coupling reaction. Steady-state fluorescence titrations and transient fluorescence measurements confirmed that this interaction prolongs the excited-state lifetime of Ir-1 and enhances its photocatalytic performance. In contrast, the Ir-PS without the pentafluorophenyl group demonstrated reduced photocatalytic activity and lower electron transfer rates. In this work, we aim to highlight that the strategic incorporation of phenyl–pentafluorophenyl interaction in dual-catalytic systems represents an effective strategy

for enhancing reaction efficiency. While previous studies have reported the utilization of hydrogen bonding or host–guest interaction to improve catalytic performance, systematic investigations on phenyl–pentafluorophenyl interaction remain scarce in such systems. We hope that this work can provide some new ideas for the construction of dual-catalytic systems. This innovative approach of leveraging intermolecular forces to strengthen the connection between the photosensitizer and catalyst shows considerable potential for advancing photocatalytic applications.

Supplementary Materials: The following supporting information can be downloaded at https://www.mdpi.com/article/10.3390/inorganics13070229/s1, Figure S1: UV-Vis spectra of four PSs (0.5 mM) in DMF; Figure S2: Steady-state emission spectra of Ni_3Ce (0.5 mM) and four PSs (0.5 mM) in DMF with 450 nm excitation; Figure S3: (a) Steady-state fluorescence quenching of Ir-1 (0.025 mM) with different concentrations of 4-methylbenzenethiol in DMF. (b) Stern–Volmer analysis of the results. The excitation wavelength is 450 nm; Figure S4. (a) Steady-state fluorescence quenching of Ir-1 (0.025 mM) with different concentrations of pyridine in DMF. (b) Stern–Volmer analysis of the results. The excitation wavelength is 450 nm; Figure S5: ESI-MS spectrum of $[Ir(coum)_2(ppipH)]^+$ in CH_3CN; Figure S6: ESI-MS spectrum of $[Ir(ppy)_2(ppipH)]^+$ in CH_3CN; Figure S7: ESI-MS spectrum of $[Ni_3Ce]^+ + 2H_2O$ in CH_3OH; Figure S8: ^1H NMR spectra of Ni_3Ce; Figure S9: ^1H NMR spectra of ppipH; Figure S10: ^1H NMR spectra of Ir-1; Figure S11: ^1H NMR spectra of Ir-2; Figure S12: ^1H NMR spectra of Ir-3; Figure S13: ^1H NMR spectra of Ir-4.

Author Contributions: Conceptualization, S.-L.H.; investigation, J.-F.C.; data curation, Z.-X.Z.; writing—original draft preparation, J.-F.C.; writing—review and editing, S.-L.H. and J.L.; project administration, S.-L.H.; funding acquisition, S.-L.H. All authors have read and agreed to the published version of the manuscript.

Funding: This work was supported by the National Science Foundation of China (21971011).

Institutional Review Board Statement: Not applicable.

Informed Consent Statement: Not applicable.

Data Availability Statement: The original contributions presented in this study are included in the article/Supplementary Materials. Further inquiries can be directed to the corresponding authors.

Acknowledgments: The technical support from the staff at the Analysis and Testing Center, Beijing Institute of Technology is also appreciated.

Conflicts of Interest: The authors declare no conflicts of interest.

References

1. Gong, J.; Li, C.; Wasielewski, M.R. Advances in solar energy conversion. *Chem. Soc. Rev.* **2019**, *48*, 1862–1864. [CrossRef] [PubMed]
2. Balzani, V.; Credi, A.; Venturi, M. Photochemical conversion of solar energy. *Chemsuschem* **2008**, *1*, 26–58. [CrossRef] [PubMed]
3. Skubi, K.L.; Blum, T.R.; Yoon, T.P. Dual Catalysis Strategies in Photochemical Synthesis. *Chem. Rev.* **2016**, *116*, 10035–10074. [CrossRef] [PubMed]
4. Wu, Q.-J.; Si, D.-H.; Ye, S.; Dong, Y.-L.; Cao, R.; Huang, Y.-B. Photocoupled Electroreduction of CO_2 over Photosensitizer-Decorated Covalent Organic Frameworks. *J. Am. Chem. Soc.* **2023**, *145*, 19856–19865. [CrossRef]
5. Gangjee, A.; Zeng, Y.; Talreja, T.; McGuire, J.J.; Kisliuk, R.L.; Queener, S.F. Design and Synthesis of Classical and Nonclassical 6-Arylthio-2,4-diamino-5-ethylpyrrolo[2,3-d]pyrimidines as Antifolates. *J. Med. Chem.* **2007**, *50*, 3046–3053. [CrossRef]
6. Le Grand, B.; Pignier, C.; Létienne, R.; Cuisiat, F.; Rolland, F.; Mas, A.; Vacher, B. Sodium Late Current Blockers in Ischemia Reperfusion: Is the Bullet Magic? *J. Med. Chem.* **2008**, *51*, 3856–3866. [CrossRef]
7. Sun, Z.-Y.; Botros, E.; Su, A.-D.; Kim, Y.; Wang, E.; Baturay, N.Z.; Kwon, C.-H. Sulfoxide-Containing Aromatic Nitrogen Mustards as Hypoxia-Directed Bioreductive Cytotoxins. *J. Med. Chem.* **2000**, *43*, 4160–4168. [CrossRef]
8. Eichman, C.C.; Stambuli, J.P. Transition Metal Catalyzed Synthesis of Aryl Sulfides. *Molecules* **2011**, *16*, 590–608. [CrossRef]
9. Sayah, M.; Organ, M.G. Potassium Isopropoxide: For Sulfination It is the Only Base You Need! *Chem. Eur. J.* **2013**, *19*, 16196–16199. [CrossRef]

10. Fernández-Rodríguez, M.A.; Shen, Q.; Hartwig, J.F. A General and Long-Lived Catalyst for the Palladium-Catalyzed Coupling of Aryl Halides with Thiols. *J. Am. Chem. Soc.* **2006**, *128*, 2180–2181. [CrossRef]
11. Hartwig, J.F. Evolution of a Fourth Generation Catalyst for the Amination and Thioetherification of Aryl Halides. *Acc. Chem. Res.* **2008**, *41*, 1534–1544. [CrossRef] [PubMed]
12. Tyson, E.L.; Ament, M.S.; Yoon, T.P. Transition Metal Photoredox Catalysis of Radical Thiol-Ene Reactions. *J. Org. Chem.* **2013**, *78*, 2046–2050. [CrossRef]
13. Oderinde, M.S.; Frenette, M.; Robbins, D.W.; Aquila, B.; Johannes, J.W. Photoredox Mediated Nickel Catalyzed Cross-Coupling of Thiols With Aryl and Heteroaryl Iodides via Thiyl Radicals. *J. Am. Chem. Soc.* **2016**, *138*, 1760–1763. [CrossRef] [PubMed]
14. Bergamaschi, E.; Weike, C.; Mayerhofer, V.J.; Funes-Ardoiz, I.; Teskey, C.J. Dual Photoredox/Cobaloxime Catalysis for Cross-Dehydrogenative α-Heteroarylation of Amines. *Org. Lett.* **2021**, *23*, 5378–5382. [CrossRef]
15. Zhang, G.; Liu, C.; Yi, H.; Meng, Q.; Bian, C.; Chen, H.; Jian, J.-X.; Wu, L.-Z.; Lei, A. External Oxidant-Free Oxidative Cross-Coupling: A Photoredox Cobalt-Catalyzed Aromatic C–H Thiolation for Constructing C–S Bonds. *J. Am. Chem. Soc.* **2015**, *137*, 9273–9280. [CrossRef]
16. Perepichka, I.; Kundu, S.; Hearne, Z.; Li, C.-J. Efficient merging of copper and photoredox catalysis for the asymmetric cross-dehydrogenative-coupling of alkynes and tetrahydroisoquinolines. *Org. Biomol. Chem.* **2015**, *13*, 447–451. [CrossRef] [PubMed]
17. Ling, B.; Yao, S.; Ouyang, S.; Bai, H.; Zhai, X.; Zhu, C.; Li, W.; Xie, J. Nickel-Catalyzed Highly Selective Radical C−C Coupling from Carboxylic Acids with Photoredox Catalysis. *Angew. Chem. Int. Ed.* **2024**, *63*, e202405866. [CrossRef] [PubMed]
18. Xuan, J.; Zeng, T.-T.; Chen, J.-R.; Lu, L.-Q.; Xiao, W.-J. Room Temperature C—P Bond Formation Enabled by Merging Nickel Catalysis and Visible-Light-Induced Photoredox Catalysis. *Chem. Eur. J.* **2015**, *21*, 4962–4965. [CrossRef]
19. Terrett, J.A.; Cuthbertson, J.D.; Shurtleff, V.W.; MacMillan, D.W.C. Switching on elusive organometallic mechanisms with photoredox catalysis. *Nature* **2015**, *524*, 330–334. [CrossRef]
20. Oderinde, M.S.; Jones, N.H.; Juneau, A.; Frenette, M.; Aquila, B.; Tentarelli, S.; Robbins, D.W.; Johannes, J.W. Highly Chemoselective Iridium Photoredox and Nickel Catalysis for the Cross-Coupling of Primary Aryl Amines with Aryl Halides. *Angew. Chem. Int. Ed.* **2016**, *55*, 13219–13223. [CrossRef]
21. Li, Y.-L.; Li, A.-J.; Huang, S.-L.; Vittal, J.J.; Yang, G.-Y. Polypyridyl Ru(ii) or cyclometalated Ir(iii) functionalized architectures for photocatalysis. *Chem. Soc. Rev.* **2023**, *52*, 4725–4754. [CrossRef] [PubMed]
22. Cheung, P.L.; Kapper, S.C.; Zeng, T.; Thompson, M.E.; Kubiak, C.P. Improving Photocatalysis for the Reduction of CO2 through Non-covalent Supramolecular Assembly. *J. Am. Chem. Soc.* **2019**, *141*, 14961–14965. [CrossRef] [PubMed]
23. Li, H.; Li, F.; Zhang, B.; Zhou, X.; Yu, F.; Sun, L. Visible Light-Driven Water Oxidation Promoted by Host–Guest Interaction between Photosensitizer and Catalyst with A High Quantum Efficiency. *J. Am. Chem. Soc.* **2015**, *137*, 4332–4335. [CrossRef]
24. Wu, Q.-J.; Si, D.-H.; Wu, Q.; Dong, Y.-L.; Cao, R.; Huang, Y.-B. Boosting Electroreduction of CO_2 over Cationic Covalent Organic Frameworks: Hydrogen Bonding Effects of Halogen Ions. *Angew. Chem. Int. Ed.* **2023**, *62*, e202215687. [CrossRef]
25. Guo, H.; Si, D.-H.; Zhu, H.-J.; Chen, Z.-A.; Cao, R.; Huang, Y.-B. Boosting CO_2 Electroreduction over a Covalent Organic Framework in the Presence of Oxygen. *Angew. Chem. Int. Ed.* **2024**, *63*, e202319472. [CrossRef] [PubMed]
26. Reichenbächer, K.; Süss, H.I.; Hulliger, J. Fluorine in crystal engineering—"the little atom that could". *Chem. Soc. Rev.* **2005**, *34*, 22–30. [CrossRef]
27. Sun, Y.; Lei, Y.; Liao, L.; Hu, W. Competition between Arene–Perfluoroarene and Charge-Transfer Interactions in Organic Light-Harvesting Systems. *Angew. Chem. Int. Ed.* **2017**, *56*, 10352–10356. [CrossRef]
28. Botta, C.; Cariati, E.; Cavallo, G.; Dichiarante, V.; Forni, A.; Metrangolo, P.; Pilati, T.; Resnati, G.; Righetto, S.; Terraneo, G.; et al. Fluorine-induced J-aggregation enhances emissive properties of a new NLO push-pull chromophore. *J. Mater. Chem. C* **2014**, *2*, 5275–5279. [CrossRef]
29. Lin, S.-M.; Velayudham, M.; Tsai, C.-H.; Chang, C.-H.; Lee, C.-C.; Luo, T.-T.; Thanasekaran, P.; Lu, K.-L. A Molecular Triangle as a Precursor Toward the Assembly of a Jar-Shaped Metallasupramolecule. *Organometallics* **2014**, *33*, 40–44. [CrossRef]
30. Han, Y.-F.; Li, H.; Jin, G.-X. Host-guest chemistry with bi- and tetra-nuclear macrocyclic metallasupramolecules. *Chem. Commun.* **2010**, *46*, 6879–6890. [CrossRef]
31. Liu, J.-X.; Zhang, X.-B.; Li, Y.-L.; Huang, S.-L.; Yang, G.-Y. Polyoxometalate functionalized architectures. *Coord. Chem. Rev.* **2020**, *414*, 213260. [CrossRef]
32. Tritton, D.N.; Bodedla, G.B.; Tang, G.; Zhao, J.; Kwan, C.-S.; Leung, K.C.-F.; Wong, W.-Y.; Zhu, X. Iridium motif linked porphyrins for efficient light-driven hydrogen evolution via triplet state stabilization of porphyrin. *J. Mater. Chem. A* **2020**, *8*, 3005–3010. [CrossRef]
33. Yoshizawa, M.; Klosterman, J.K.; Fujita, M. Functional Molecular Flasks: New Properties and Reactions within Discrete, Self-Assembled Hosts. *Angew. Chem. Int. Ed.* **2009**, *48*, 3418–3438. [CrossRef]
34. Syntrivanis, L.-D.; Tiefenbacher, K. Reactivity Inside Molecular Flasks: Acceleration Modes and Types of Selectivity Obtainable. *Angew. Chem. Int. Ed.* **2024**, *63*, e202412622. [CrossRef]

35. Xue, R.; Liu, Y.-S.; Huang, S.-L.; Yang, G.-Y. Recent Progress of Covalent Organic Frameworks Applied in Electrochemical Sensors. *ACS Sens.* **2023**, *8*, 2124–2148. [CrossRef] [PubMed]
36. Nagae, H.; Sakamoto, K.; Fujiwara, S.; Schindler, T.; Kon, Y.; Sato, K.; Okuda, J.; Mashima, K. Aerobic oxygenation of α-methylene ketones under visible-light catalysed by a $CeNi_3$ complex with a macrocyclic tris(salen)-ligand. *Chem. Commun.* **2021**, *57*, 11169–11172. [CrossRef]
37. Chen, W.; Chen, Y.; Li, J.; Zhang, S.; Zhang, D.; Li, D.; Wang, S.; Yu, F.; Chen, Y.; Zhang, J. Layer stacked polyimide with great built-in electronic field for fast lithium-ion storage based on strong p-p stacking effect. *Energy Storage Mater.* **2024**, *68*, 103349. [CrossRef]
38. Takizawa, S.-y.; Pérez-Bolívar, C.; Anzenbacher, P., Jr.; Murata, S. Cationic Iridium Complexes Coordinated with Coumarin Dyes—Sensitizers for Visible-Light-Driven Hydrogen Generation. *Eur. J. Inorg. Chem.* **2012**, *2012*, 3975–3979. [CrossRef]
39. Sebata, S.; Takizawa, S.-y.; Ikuta, N.; Murata, S. Photofunctions of iridium(iii) complexes in vesicles: Long-lived excited states and visible-light sensitization for hydrogen evolution in aqueous solution. *Dalton Trans.* **2019**, *48*, 14914–14925. [CrossRef]

Disclaimer/Publisher's Note: The statements, opinions and data contained in all publications are solely those of the individual author(s) and contributor(s) and not of MDPI and/or the editor(s). MDPI and/or the editor(s) disclaim responsibility for any injury to people or property resulting from any ideas, methods, instructions or products referred to in the content.